4

Particle beams

Most particle physics experiments require a beam of particles of a certain type. Usually these particles are provided by a high energy accelerator. Thus we will begin this chapter with a brief description of the characteristics of particle accelerators. These divide into two major classes, depending on whether the particle beam collides with a fixed target or with another beam of particles. We then discuss some properties of secondary beams from fixed target accelerators and the rudiments of beam transport theory. Since an important property of the beam for the experimentalist is the intensity, we will discuss flux monitoring. This is followed by a description of alternate sources of particles. The chapter concludes with a discussion of radiation protection.

4.1   Particle accelerators

A particle experimentalist is primarily concerned with four properties of the particle beam: the energy, the flux of particles, the duty cycle of the accelerator, and the fine structure in the intensity as a function of time. The duty cycle is defined to be the fraction of the time that the accelerator is delivering particles to the experiment. A detailed description of the components and acceleration process in various types of accelerators is beyond the scope of this book [1, 2]. However, we will give a brief overview in order to introduce some of the terminology.

The beam in an accelerator starts in either an electron gun or an ion source. Electrons are liberated from the filament of a high voltage triode tube. Pulses $1-10\,\mu$s long can be produced at a repetition rate of up to 500 Hz by triggering the grid of the tube. Electrons leave the source with $\beta \sim 0.5$. Protons originate from hydrogen molecules, which are dissociated with radio frequency (rf) energy into atoms. In a typical proton ion

source, electrons oscillate back and forth inside the chamber. Collisions with neutral molecules and atoms result in the production of positive ions. These are attracted to the outlet port by an electric field and formed into a jet with a circular nozzle. Typically the output current is several milliamperes and the beam energy is several keV.

The beam from the source goes through several intermediate stages prior to injection into the main accelerating structure. For efficient injection the energy of the beam leaving an ion source must be increased. In the past this has usually been done for protons with a Cockcroft–Walton potential drop accelerator. The Cockcroft–Walton is essentially a voltage doubler circuit that can be repeated many times. The ions are accelerated by the potential differences between the stages and can reach an energy of up to 1 MeV. Electrical potential drop accelerators are ultimately limited by arcing and corona discharge. Recently the Cockcroft–Walton stage of some accelerators has been replaced with a radio frequency quadrupole (RFQ). This device can simultaneously accelerate, focus, and bunch a beam of particles.

Existing particle accelerators may be broadly classified into two groups: fixed target accelerators and storage rings. The beam in a fixed target accelerator is accelerated to its operating energy and then extracted. The beam in a storage ring, on the other hand, is accelerated to the desired energy and maintained in the ring for as long a period as possible.

4.1.1   Fixed target accelerators

Table 4.1 contains a summary of some important properties of existing fixed target accelerators with a maximum beam energy of 10 GeV or more. The chief advantages of this type of accelerator are the large number of interactions that occur when the extracted beam is directed into a liquid or solid target, and the fact that the particles emerge in the forward direction so that the required detector solid angle coverage is small.

Fixed target accelerators can be further divided into linear and circular accelerators. A linear accelerator (or linac) consists of an evacuated waveguide with a periodic array of gaps or cavities. High frequency oscillators establish an electromagnetic wave in the structure. The beam is forced into bunches and there may be rapid variations in the intensity of the extracted beam (rf structure) if it is not properly debunched. Linacs are frequently used as preaccelerators for synchrotrons. The largest linac currently in operation is the 2-mile-long electron accelerator at the Stanford Linear Accelerator Center (SLAC). It typically produces a 22-GeV

Table 4.1. *Fixed target accelerators*

Accelerator	Location	Date of first operation	Accelerated particles	Circumference (m)	M be (C
KEK	Japan	1976	p	339	
SLAC	United States	1966	e⁻	3050[a]	
CERN PS	Europe	1959	p	628	
AGS	United States	1961	p	807	
Serpukhov	USSR	1967	p	1484	
Fermilab	United States		p	6280	
Main Ring		1972			
Tevatron II		1983			1(
CERN SPS	Europe	1976	p	6910	

[a] Linac.
[b] For 1.7-μs bursts.
Source: M. Crowley-Milling, Rep. Prog. Phys. 46: 51, 1983; R. Wilson, Sci. Amer., Jan. 1980, p

beam with a train of ~ 5000 bunches of 1.6-μs pulses and a repetition rate of up to 180 Hz.

The high energy acceleration mechanism in all existing electron and proton machines relies on forcing the particles to travel through an electric field. In electron linacs a traveling electromagnetic wave can be created that has a longitudinal component of electric field moving in phase with the particles. So long as this phase relationship can be maintained, the electrons will continue to be accelerated. Proton linacs often use the scheme illustrated in Fig. 4.1. The linac contains a series of drift tubes separated by gaps. The drift lengths are arranged so that the bunch of protons crosses the centers of the accelerating gaps at the same time that the field across the gap is approximately maximum, causing the particles to be continuously accelerated.

The synchrotron is a cyclic machine in which the particle beam is confined to a closed orbit by a series of bending magnets around a ring. The momentum p of a particle with charge q moving with a radius of curvature ρ in a magnetic field B is

$$p = qB\rho \qquad (4.1)$$

For singly charged particles the momentum (in GeV/c) is given by $p = 0.3B\rho$, where B is in tesla and ρ is in meters. On each pass around the ring the particles' momenta are increased by acceleration in a synchronized rf cavity. As the momentum increases, the magnetic field in the bending magnets has to be increased to keep ρ constant. Particles in the beam

Figure 4.1 Principle of acceleration in a proton linac. A particle bunch is shown at $t = 0$ in an accelerating gap where the longitudinal component of the electric field is maximum. If the electric field phase is properly adjusted, the field will also be a maximum when the particle reaches the next gap. Between gaps the bunch must be shielded from the field.
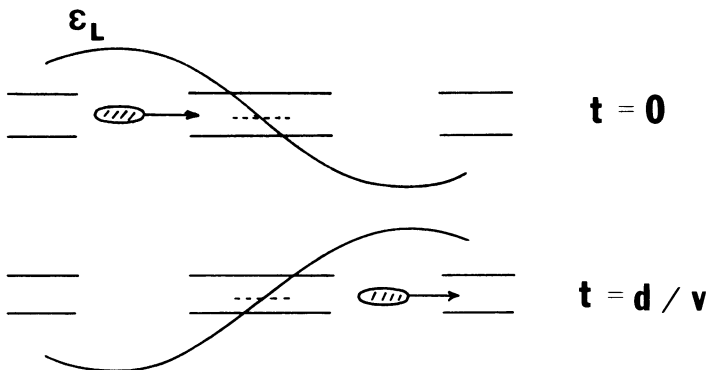
undergo transverse spatial (betatron) oscillations and energy (synchro-tron) oscillations, which become smaller as the energy is increased. Quadrupole magnets are used to keep the beam focused.

Proton beams are accelerated to high energy in a synchrotron. Figure 4.2 shows the layout of the beams at the Fermilab (FNAL) accelerator [3]. This is the first large accelerator built with superconducting magnets. The linac accelerates the proton beam to 200 MeV. This is followed by a booster, which stores the linac output pulse and accelerates it to 8 GeV in $\frac{1}{15}$ sec. A series of booster pulses are injected into the main accelerator ring before the acceleration cycle begins. Each time the beam crosses the rf cavities, it gains 2.8 MeV of energy.

The acceleration cycle of a typical fixed target accelerator is shown in Fig. 4.3. Once the machine reaches peak energy, the magnetic field in the

Figure 4.2 Secondary beamlines at the Tevatron. (Courtesy of Fermi National Accelerator Laboratory.)
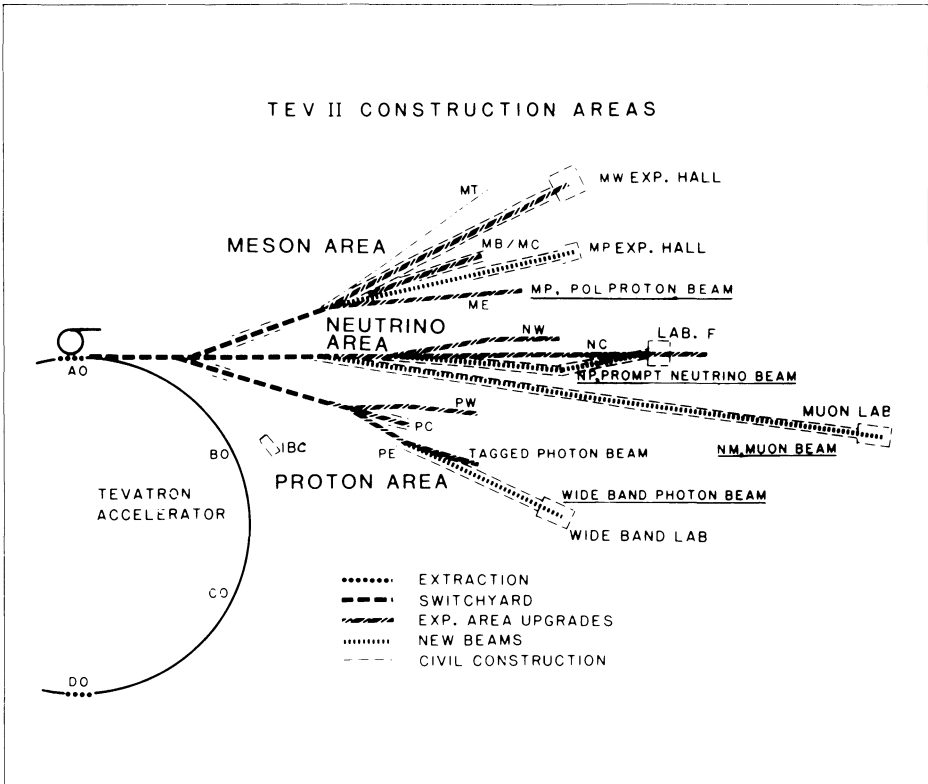
ring bending magnets can be held fixed for a period of around 1 sec (flat top), while the beam is slowly extracted from the machine for counter experiments. Alternatively, the beam can be extracted quickly for bubble chamber of neutrino experiments. The extracted FNAL beam has a peak energy of $\sim 1000\,\mathrm{GeV}$ (Tev II) and an intensity of 2×10^{13} protons/pulse. The field is then lowered and the acceleration cycle is repeated. The beam size shrinks by a factor of about 10 between injection and extraction. The primary extracted proton beam is sent through a target "switchyard," which delivers beams to three major experimental areas: proton, meson, and neutrino.

The circular acceleration of electrons is severely hampered because of synchrotron radiation. The energy lost to radiation per revolution is [4]

$$\Delta E = (4\pi e^2/3\rho)\beta^3\gamma^4 \tag{4.2}$$

where ρ is the radius of the orbit. For electrons with $\beta \sim 1$, the energy loss in keV is $88.5E^4/\rho$, where E is in GeV and ρ is in meters. This lost energy must be replaced by the rf cavities on each revolution. The emitted radiation at high energy lies in a small cone around the particles' direction with an opening angle that goes like $1/\gamma$. The energy is deposited in a narrow strip around the circumference of the machine.

Figure 4.3 Acceleration cycle at a fixed target accelerator. (1) injection, (2) acceleration, (3) flat top and extraction, (4) deceleration.
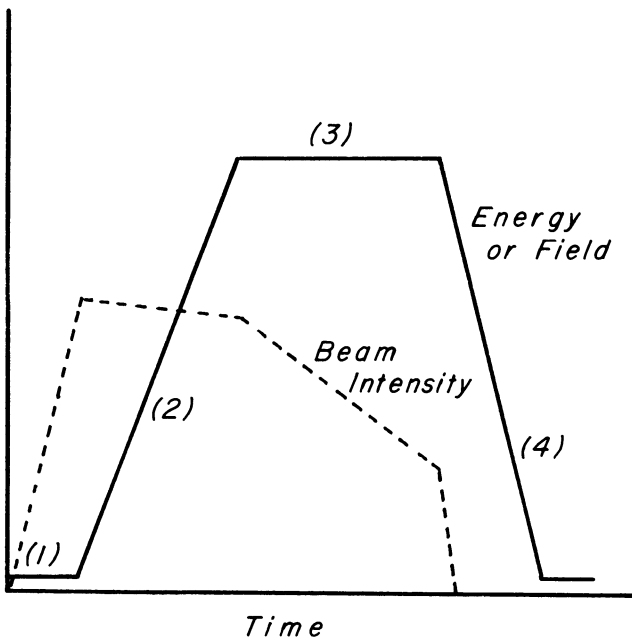
It is possible to accelerate polarized beams of particles. This is accomplished for protons by preparing and then selecting specific atomic states in the source [5]. Electron and positron beams in circular machines tend to polarize themselves in the vertical direction via the process of synchrotron radiation emission [6]. The theoretical maximum polarization arising from this (Sokolov – Ternov) effect is 92%. Electrons in linear accelerator sources can be polarized by exciting transitions in crystals using circularly polarized laser light [7]. The acceleration of polarized particles is complicated by the existence of depolarizing resonances, which occur at certain values of the particle's momentum. Most polarized sources can only produce a fraction of the intensity of an unpolarized source.

4.1.2 Storage ring accelerators

The center of mass energy available at fixed target accelerators is given by ($c = 1$)

$$E^* = (m_b^2 + m_t^2 + 2m_t E_b)^{1/2} \tag{4.3}$$

where m_b (m_t) is the beam (target) particle mass and E_b is the beam energy in the LAB frame. At high energy

$$E^* \simeq (2m_t E_b)^{1/2} \tag{4.4}$$

Thus, the available energy for the production of particles only increases as the square root of the beam energy. Energy is more readily available in a colliding beam machine, where two beams of circulating particles are made to interact head on. Here the LAB and the CM systems are the same and we find that

$$E^* = 2E_b \tag{4.5}$$

If the beams have variable energies E_1 and E_2 and cross at an angle α, the CM energy at high energy is

$$E^* \simeq 2(E_1 E_2)^{1/2}\cos(\tfrac{1}{2}\alpha) \tag{4.6}$$

Table 4.2 summarizes some characteristics of existing storage rings with a maximum energy per beam of 4 GeV or more.

A useful measure of storage ring performance is the luminosity $\mathcal{L}$. The reaction rate R is given in terms of $\mathcal{L}$ by

$$R = \mathcal{L}\sigma \tag{4.7}$$

where σ is the cross section for the reaction under consideration. Thus, luminosity has the dimensions of particles/s-cm². If two bunches of N particles are circling the machine with frequency f, the luminosity at an intersection point is

$$\mathcal{L} = N^2 f/A \tag{4.8}$$

Table 4.2. *Colliding beam accelerators*

Accelerator	Location	Date of operation	Stored particles	Circumference (m)	Interse regions
SPEAR	SLAC, United States	1972	e^+e^-	234	2
DORIS II	DESY, Germany	1982	e^+e^-	288	2
VEPP-4	Novosibirsk, USSR	1978	e^+e^-	366	3
CESR	Cornell, United States	1979	e^+e^-	768	2
PEP	SLAC, United States	1980	e^+e^-	2200	6
PETRA	DESY	1978	e^+e^-	2304	6
ISR[a]	CERN, Europe			942	8
		1971	pp	—	—
		1980	$\mathrm{p\bar{p}}$		
S$\mathrm{\bar{p}}$pS	CERN	1981	$\mathrm{p\bar{p}}$	6910	2

[a] Decomissioned in 1984.

Source: M. Crowley-Milling, Rep. Prog. Phys. 46: 51, 1983; R. Wilson, Sci. Amer., Jan. 1980, p. 4: Part. Sci. 33: 67, 1983.

where A is the effective cross-sectional area of beam overlap. If two un-equal Gaussian beams are bunched with k bunches per revolution in each beam, the luminosity is [8]

$$\mathcal{L} \simeq \frac{fkN_1N_2}{4\pi a_h a_v} \tag{4.9}$$

where N_i is the number of particles per bunch and a_h, a_v are the rms horizontal and vertical dimensions. For horizontal crossing

$$a_h = (a_r^2 + \alpha^2 a_b^2)^{1/2}$$

where a_b is the rms bunch length, a_r is the radial bunch dimension, and α is the crossing angle.

The electron–positron storage ring capable of reaching the highest CM energy at present is PETRA, with energies around 23 GeV per beam and luminosities of 10^{31} particles/s-cm^2. Positive and negative beams can be stored in a single ring and made to cross only at fixed intersection regions. Proton–proton storage rings require the use of two separate rings. The largest pp storage ring was the ISR with an energy of 31 GeV per beam and a luminosity of 4×10^{31} particles/s-cm^2. The beams in e^+e^- rings are tightly bunched, whereas the proton beams in the ISR were more nearly continuous. For comparison, the equivalent luminosity of a fixed target accelerator beam of $\sim 10^{13}$ particles/sec incident on 1 m of liquid hydrogen is 4×10^{37}/s-cm^2.

The design requirements for storage rings are more stringent than for fixed target machines, since the beams must be confined for periods of hours or more. The vacuum in the rings is typically 10^{-8} torr or less to prevent beam–gas interactions from limiting the lifetime of the beam. The maximum luminosity is limited by coupling of one beam with the other, space charge repulsion of the particles in each beam, and instabilities in the beam orbits [6].

The use of antiprotons in storage rings requires additional efforts to raise the luminosity to usable levels. The $\bar{p}$ are produced by proton inter-actions in a solid target. Those $\bar{p}$ produced in a particular solid angle and within a certain momentum interval can be accumulated in a ring. However, it is necessary to increase the density of the accumulated beam before it is accelerated and collided. This is accomplished by "cooling" the beam [9]. Two types of cooling are commonly used. In electron cooling an electron beam is injected into a straight section of the ring with the same velocity as the $\bar{p}$. Coulomb collisions between the two beams damp the transverse oscillations of the heavier $\bar{p}$. In stochastic cooling pickup electrodes on one side of the ring measure deviations of a small

circumferential portion of the beam from the equilibrium orbit. A correction signal is then sent directly across the ring, so that kicker magnets can apply a correlation deflection to the beam portion when it arrives on the opposite side of the ring. Stochastic cooling can also be used to reduce the momentum spread in the beam. These cooling techniques make it possible to increase the luminosity in $\bar{p}p$ machines to useful levels.

Figure 4.4 shows part of the accelerator complex at CERN. The heart of the system is the 28-GeV proton synchrotron (PS). The extracted PS beam can be used for low energy experiments or injected into one of the higher energy machines, the SPS or ISR. The SPS can be used either as a 400-GeV proton synchrotron or as a 315 on 315-GeV $\bar{p}p$ collider. The antiprotons are produced in 26-GeV/c proton collisions with a fixed target. The collected $\bar{p}$ are cooled and stored in an accumulator ring at 3.5 GeV/c. Then they can be reaccelerated in the PS and injected into either the ISR or SPS. Experiments with high quality beams of low energy $\bar{p}$ can be performed at the LEAR storage ring.

A number of new colliding beam accelerators are presently under construction. Table 4.3 lists six major projects that should be completed within the next few years. These include circular e^+e^- colliders (LEP and TRISTAN), a linear e^+e^- collider (SLC), a new $\bar{p}p$ collider (Tevatron I), and an e^-p collider (HERA).

Figure 4.4 Layout of part of the CERN accelerator complex. (A) linac, (B) LEAR storage ring, (C) $\bar{p}$ production target, and (D) antiproton accumulator. (Assisted by CERN.)
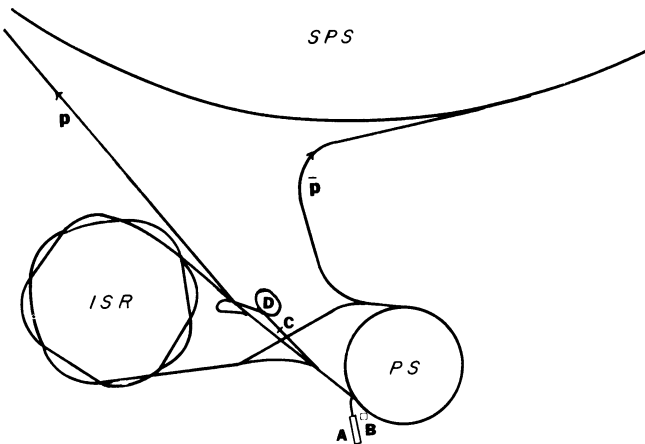
4.2 Secondary beams

Secondary beams at fixed target accelerators are created by sending a portion of the primary extracted beam into a target. Many different particles will be created, each with its own characteristic angle and momentum spectrum. A typical beamline starts with a collimator to select particles produced in some specific angular range. This is a narrow restriction built from lead bricks or other materials, which reduces the intensity or divergence of the beam or selects particles going in a specific direction.

A useful device for separating particles by mass in a low energy charged beam is the electrostatic separator. The electric portion of the Lorentz force gives a momentum kick to each particle that is proportional to the length of time the particle spends inside the separator. Since particles with different masses but the same momentum move with different velocities, they will spend different lengths of time in the separator and will spread out transversely at the end of the device. A judiciously placed slit will then permit the desired component of the beam to be passed on.

The deflection angle away from the axis is given by ($c = 1$)

$$\alpha = \frac{\Delta p_\perp}{p_0} = \frac{L}{\beta p_0}(e\beta B - e\mathcal{E})$$

where L is the length of the separator, β is the velocity, p_0 is the beam momentum, B is an applied magnetic field, and $\mathcal{E}$ is the applied electric field. Writing $\mathcal{E}$ in terms of the electrical potential V and the plate separation d gives

$$\alpha = \frac{eL}{p_0}\frac{V}{d}\left(\frac{1}{\beta_0} - \frac{1}{\beta}\right) \tag{4.10}$$

Table 4.3. *Major construction projects*

Project	Location	Estimated completion date	Description
LEP	CERN	1988	50 GeV $\times$ 50 GeV e^+e^- collider
SLC	SLAC	1987	50 GeV $\times$ 50 GeV e^+e^- linear collider
Tevatron I	Fermilab	1986	1 TeV $\times$ 1 Tev $\bar{p}p$ collider
TRISTAN	KEK	1986	30 GeV $\times$ 30 GeV e^+e^- collider
HERA	DESY	1990	30 GeV-electron $\times$ 820 GeV-proton collider
UNK	Serpukhov	1990	600-GeV proton Synchrotron

where β_0 is the velocity for no deflection. Note that the purpose of the magnetic field is to determine the velocity β_0 that will pass through undeflected, where

$$\beta_0 = \mathcal{E}/B \tag{4.11}$$

Using the expression $p = \beta E$, we can rewrite Eq. 4.10 as

$$\alpha = \frac{eLV}{p_0 d} \left[\left(1 + \frac{m_0^2}{p_0^2}\right)^{1/2} - \left(1 + \frac{m^2}{p^2}\right)^{1/2} \right] \tag{4.12}$$

When $p \simeq p_0 \gg m$,

$$\alpha = \frac{eLV}{p_0 d} \frac{1}{2} \frac{m_0^2 - m^2}{p_0^2} \tag{4.13}$$

Thus, at high energy the deflection angle decreases like $1/p_0^3$, and this means of separation is only practical up to about 5 GeV/c momentum. The major difficulty is the large electric field required, typically 30 kV/cm. Separation can also be accomplished using rf fields [10].

We will now consider some of the important features of various secondary beams.

4.2.1 γ

Photon beams can be created directly from an electron beam by bremsstrahlung or from a proton beam via π^0 decays. Charged particles are removed from the beam using collimators and bending magnets. A significant fraction of the neutral beam may consist of neutrons. The γ to n ratio may be improved by passing the beam through a material such as liquid deuterium, whose nuclear interaction length is significantly shorter than its radiation length. The beam contamination can be estimated by inserting lead absorbers and purposely decreasing the γ content of the beam.

The energy of the γ can be determined in a tagged photon beam. This is usually accomplished by sending an electron beam whose energy is well measured into a thin, high Z target as shown in Fig. 4.5. After the photon is created via bremsstrahlung, the electron's energy is remeasured and the photon energy determined from energy conservation. As an example, the tagged photon beam at the Omega Spectrometer at CERN uses 4×10^{12} incident 240-GeV protons to produce 2×10^7 electrons per pulse [11]. This results in $\sim 10^6$ tagged photons in the momentum range 25–70 GeV/c. The spectrum falls off with the expected p_γ^{-1} dependence. Photon beams can be polarized by production from crystals or selective absorption.

4.2.2 ν_μ, ν_e, $\bar{\nu}_\mu$, $\bar{\nu}_e$

Most neutrino beams originate in the decays of charged pions and kaons. Muon neutrino beams are produced in the 2-body decays

$$\pi^+ \rightarrow \mu^+\nu_\mu$$
$$\pi^- \rightarrow \mu^-\bar{\nu}_\mu$$
$$K^+ \rightarrow \mu^+\nu_\mu$$
$$K^- \rightarrow \mu^-\bar{\nu}_\mu$$
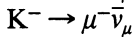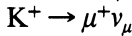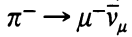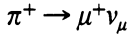
Electron neutrinos are produced in the 3-body decays

$$K^+ \rightarrow e^+\pi^0\nu_e$$
$$K^- \rightarrow e^-\pi^0\bar{\nu}_e$$
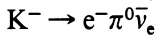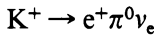
The ν_e fluxes are suppressed by ~ 100 times compared to the ν_μ fluxes. A neutrino beamline typically consists of a thin production target where the π and K are produced, a decay region, and a long earth absorber where hadrons and decay muons are absorbed.

There are two general types of neutrino beams [12]. In a wide band beam the π and K are collected over a wide range of momenta and solid angle. The resultant beam has a high neutrino flux, but the energy spectrum is very broad. Sometimes a horn is used to increase the intensity. This is a thin metal sheet that surrounds the beamline after the production target. When a large current pulse is sent through the horn, the azimuthal magnetic field focuses π and K of a given charge into a parallel beam toward the detector. The oppositely charged mesons are defocused. As a result, the meson decay product beam consists primarily of neutrinos or primarily of antineutrinos. The horn-focused energy spectrum is strongly peaked at small neutrino energy. Sometimes instead of a horn a quadru-

Figure 4.5 Principle of the tagged photon beam. (e) electron beam, (C) collimators, (BM) bending magnets, (R) radiator, and (T) tagging counters.
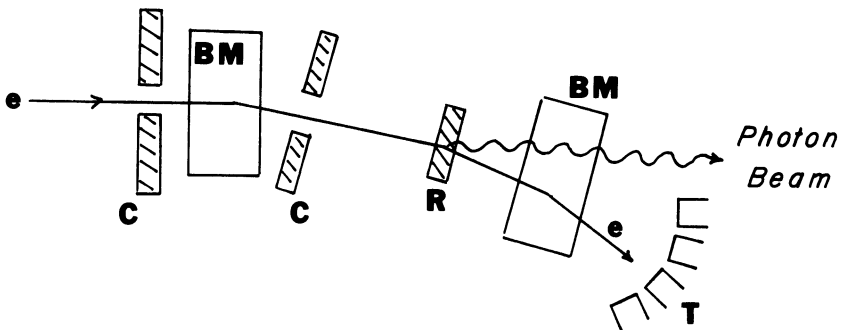
pole triplet is used to focus the mesons. The flux of 100-GeV neutrinos from the horn-focused beam at FNAL is around 2×10^6 per 10^{13} incident 400-GeV protons per m^2.

In a narrow band beam the mesons are momentum-selected before entering the decay region. The neutrinos in such a beam have a much tighter energy spectrum ($\sigma_E/E \sim 20\%$). Figure 4.6 shows the Fermilab narrow band ν spectrum. The spectrum is dichromatic with peaks corresponding to the 2-body π and K decays. The integrated intensity is much smaller than in the broad band beam. The decay angle of the neutrino is correlated with its energy.

4.2.3 $e^{\pm}$

A secondary e^+ or e^- beam can be created at a proton machine by producing π^0 in a thin production target. The decay photons can be converted in a thin radiator to yield $\pi^0 \rightarrow 2\gamma \rightarrow 2e^+ + 2e^-$.

Figure 4.6 Fermilab narrow band neutrino flux for 200-GeV π and K secondary beams. (H. Fisk and F. Sciulli, reproduced with permission from the Annual Review of Nuclear and Particle Science, Vol. 32, © 1982 by Annual Reviews, Inc.)
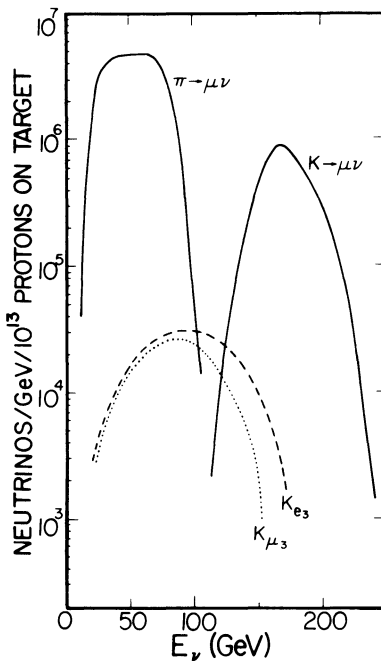
4.2.4 $\mu^{\pm}$

Muon beams are used for high energy lepton – hadron interaction studies [13]. Muon beams can be made with higher energies and intensities for these studies than electron beams can. Because of their higher mass, muon beams can be used with longer targets and have smaller, higher-order QED corrections than electrons.

A typical beam starts by first directing a secondary proton beam into a production target to create a beam of charged pions. The pions are allowed to decay until a significant fraction of the beam contains muons. Since this reaction is also used to create neutrinos, the two beams can both originate from the same decay region. The beam is then passed through a thick hadron absorber. This consists of a low Z material, such as polyethylene, in order to minimize multiple scattering of the muons. The muons readily pass through the absorber. The resulting beam has a large halo, which can, however, be significantly reduced by incorporating magnetic bending into the beamline. The 100-GeV muon beam at the SPS was created by using 400-GeV protons to produce 115-GeV pions. The μ^+ yield per proton incident on one interaction length of beryllium was 1.9×10^{-5}. A possible background consists of electrons from muon decays after the hadron absorber.

4.2.5 $\pi^{\pm}$, $K^{\pm}$, p, $\bar{p}$

High intensity proton beams are available by splitting off a portion of the primary beam at proton accelerators. Secondary beams of charged hadrons are produced by interactions of the primary beam in a nuclear target. Only particles of a given charge and produced within a certain solid angle and momentum interval will be transported down the beamline. As an example, the M1 beamline at FNAL contained 83.5% p/14.0% π^+/2.5% K^+ when the machine operated at 400 GeV [14]. The negative beam contained 95.7% π^-/3.5% K^-/0.8% $\bar{p}$. It was possible to increase the K^+ fraction of the positive beam to 15% by using a beryllium filter in the beam. At low energy the fraction of K and $\bar{p}$ in a hadron beam can be enhanced using electrostatic separators.

4.2.6 K^0, n, $\bar{n}$

Long-lived neutral hadronic beams can be made by following the production target with a thin radiator to convert photons. This in turn is followed by collimators and bending magnets to sweep all the charged particles from the beam. One obvious feature of any neutral beam is that it

must point straight back to the secondary production target. Typically, the neutron content of the beam is several orders of magnitude larger than the K^0 content, unless specific absorbers are used to enhance the K^0 fraction.

4.2.7 Λ, $\Sigma^\pm$, Ξ^-, Ξ^0, Ω^-

Hyperons are also produced at the secondary production target. At low energy it is difficult to make beams of these particles, since their mean free path for decay is only several centimeters. However, we have seen in Eq. 1.12 that the mean free path grows with momentum. This fact has allowed useful hyperon beams to be constructed at the SPS and at FNAL [15]. Charged and neutral beams may be constructed as discussed above.

4.3   Beam transport

It is important to understand how the size and angular divergence of a beam changes as it is transported from the accelerator to an experimental area. Let us begin by briefly considering the ideal motion of a particle in a magnetic field. Consider a particle with mass m, momentum p, and charge q traveling along the z axis. If a magnetic field $\mathbf{B}$ is present, the particle is subjected to the Lorentz force $\mathbf{F} = q\mathbf{v} \times \mathbf{B}$. Assume that the field $\mathbf{B}$ has the components $(B_x, B_y, 0)$. Then the equations of motion are

$$\frac{d^2x}{dz^2} + \frac{q}{p} B_y = 0 \qquad \frac{d^2y}{dz^2} - \frac{q}{p} B_x = 0 \qquad v = \text{const} \qquad (4.14)$$

where we have used $v = dz/dt$.

We now consider three important cases.

1. *Drift space.* If no field is present, the equation for x reduces to

$$x = x_0' z + x_0 \qquad (4.15)$$

where x_0 and x_0' are constants. A similar equation applies to the motion in y.

2. *Bending magnet.* Now consider an ideal bending magnet or dipole with $B_x = 0$ and $B_y = B$. For the moment we neglect the presence of the fringe field at the edges of the magnet. If we consider the equations as a function of time, the coupled equations have the solution

$$\begin{aligned} x &= r \cos(\omega t) \\ z &= r \sin(\omega t) \\ \omega &= qB/m \end{aligned} \qquad (4.16)$$

as can be verified by direct substitution. These are, of course, just the parametric equations for a circle of radius *r*.

3. *Quadrupole field.* The quadrupole field shown in Fig. 4.7 is generated by a four-pole magnet with alternating polarity. The field is of the form $\mathbf{B} = (Gy, Gx, 0)$, where the constant G is called the gradient of the quadrupole and has dimensions tesla/m. We assume in the lowest-order approximation that the particle continues to travel parallel to the *z* azis. The equations of motion become

$$\frac{d^2x}{dz^2} + \frac{q}{p}\,Gx = 0$$

$$\frac{d^2y}{dz^2} - \frac{q}{p}\,Gy = 0$$

(4.17)

Figure 4.7 Quadrupole magnetic field. The field vanishes on the axis. (C) one of the coils and (P) one of the iron pole faces. Dotted lines show equipotentials. (Assisted by Rutherford Appleton Laboratory.)
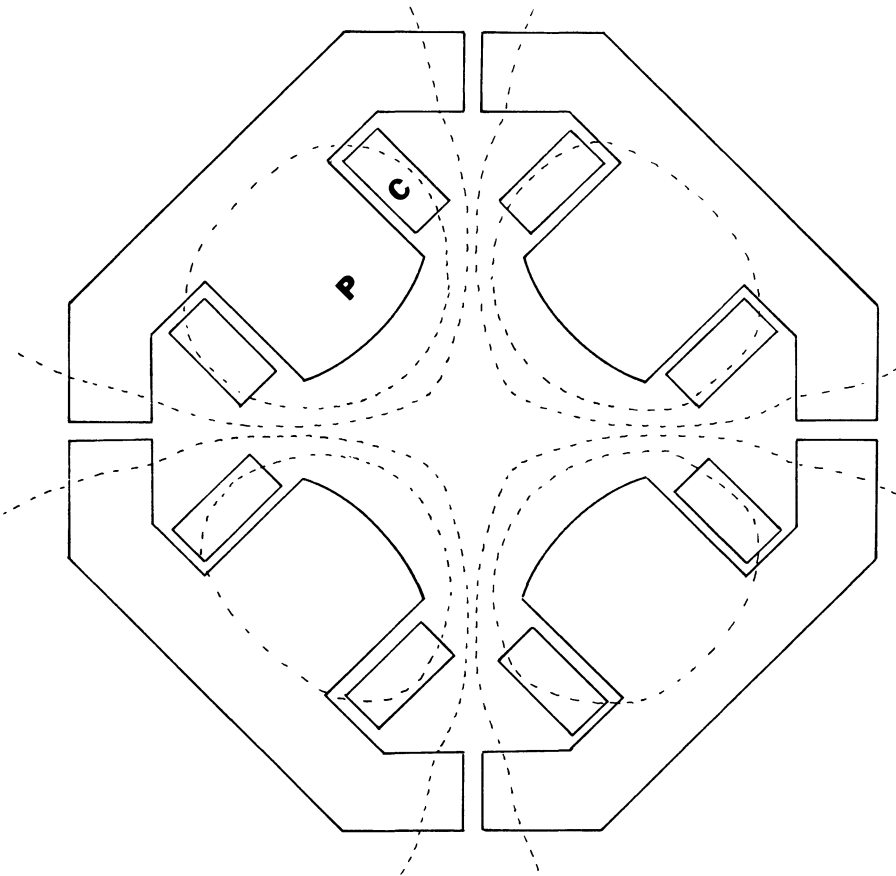
Let

$$k^2 = \frac{q|G|}{p} \tag{4.18}$$

Then the solution for the x motion is

$$x = x_0 \cos(kz) + \frac{x_0'}{k} \sin(kz) \tag{4.19}$$

which represents oscillatory motion. The solution for y,

$$y = y_0 \cosh(kz) + \frac{y_0'}{k} \sinh(kz) \tag{4.20}$$

blows up exponentially. Thus, the quadrupole has the property of focusing a beam in one direction while defocusing it in the other. Another quadrupole with the pole polarities reversed would focus in y and defocus in x. Note that the first-order equations given here do not couple the motion in x and y.

It is convenient to combine the displacement and angular divergence of a beam into the components of a 2-dimensional vector

$$\mathbf{x} = \begin{pmatrix} x \\ x' \end{pmatrix}$$

Then the action of various devices, such as quadrupole magnets or drift spaces, can be considered to be represented by matrices M_i, which operate on an initial vector $\mathbf{x}_0$ to produce the vector $\mathbf{x}$ at the end of the device. Sometimes 3-dimensional vectors are used with the momentum dispersion as the third component.

The drift space of length L has the matrix

$$M_1 = \begin{pmatrix} 1 & L \\ 0 & 1 \end{pmatrix} \tag{4.21}$$

as can be seen from Eq. 4.15.

The displacement $\mathbf{x}$ is considered to be the distance from a central, ideal orbit. In a bending magnet with field B, the entrance angle β_i and the exit angle β_o are related by

$$\sin \beta_i + \sin \beta_0 = \frac{\int B \, dl}{3.333 p_0} \tag{4.22}$$

where p_0 is the momentum of the central orbit (or ray) and the units are tesla, meters, and GeV/c. For small β_i and β_0 this can be approximated by

$$\alpha \simeq \frac{\int B \, dl}{3.333 p_0} \tag{4.23}$$

where α is the total angle of bend. The radial deviations from the central ray are given by [16]

$$M_2 = \begin{pmatrix} \cos \alpha & \rho_0 \sin \alpha \\ -\dfrac{1}{\rho_0} \sin\alpha & \cos \alpha \end{pmatrix} \tag{4.24}$$

where ρ_0 is the radius of curvature of the central orbit. Any momentum dispersion in the beam produces the additional correction

$$\frac{\Delta p}{p} \begin{pmatrix} \rho_0 \left(1 - \cos \alpha\right) \\ \sin \alpha \end{pmatrix}$$

which must be added to x. A more complete treatment must also take into account the nonuniformity of the field and the focusing by the fringe fields [16].

A quadrupole magnet behaves much like a thick optical lens. We can rewrite Eq. 4.19 for the focusing direction in terms of

$$M_3 = \begin{pmatrix} \cos kL & 1/k \sin kL \\ -k \sin kL & \cos kL \end{pmatrix} \tag{4.25}$$

and Eq. 4.20 for the defocusing direction in terms of

$$M_4 = \begin{pmatrix} \cosh kL & 1/k \sinh kL \\ k \sinh kL & \cosh kL \end{pmatrix} \tag{4.26}$$

where k is given by Eq. 4.18. In the thin lens approximation the quadrupole causes a change in the divergence of the beam that is proportional to the displacement from the central orbit,

$$\Delta x' = x/f \tag{4.27}$$

but leaves the position unchanged. Here f is the focal length of the lens. In this case we have

$$M_3' \simeq \begin{pmatrix} 1 & 0 \\ -k^2 L & 1 \end{pmatrix} \tag{4.28}$$

$$M_4' \simeq \begin{pmatrix} 1 & 0 \\ k^2 L & 1 \end{pmatrix} \tag{4.29}$$

Comparing Eqs. 4.27, 4.28, and 4.29, we see that the focal length of the thin lens is

$$f = \pm \frac{p_0}{q|G|L} \tag{4.30}$$

where a negative focal length means focusing and a positive focal length means defocusing. Sometimes the lens power $P = 1/f$ is used instead of

the focal length. A pair of quadrupoles with opposite gradients can be designed to focus in both x and y simultaneously. However, the focal lengths will be different in the horizontal and vertical directions.

Each of the transfer matrices discussed so far has unit determinant. This is a consequence of Liouville's theorem in statistical mechanics [16]. If the beamline consists of several types of devices, the overall transfer matrix can be determined by taking the product of the individual matrices.

As an example, Fig. 4.8 shows the maximum horizontal and vertical extent (beam profiles) for a medium energy separated beam. In the figure Q1 – Q8 are quadrupoles, D1 – D4 are bending dipoles, and BS1 and BS2 are electrostatic separators. The beamline accepts particles produced in a narrow solid angle near the primary beam direction. Collimator C1 can be used to adjust the particle intensity. The dipole D1 disperses the beam horizontally for subsequent momentum analysis. Quadrupoles Q1 – Q3 make the vertical beam parallel for the separators and focus the beam horizontally at the collimator C2 for momentum selection. The beam separators give a vertical divergence to the beam depending on the particle's mass. Quadrupoles Q4 and Q5 focus the beam vertically at the mass

Figure 4.8 Beam profiles for a medium energy separated beam. The beamline is shown from the production target T1 to the experimental target T2.
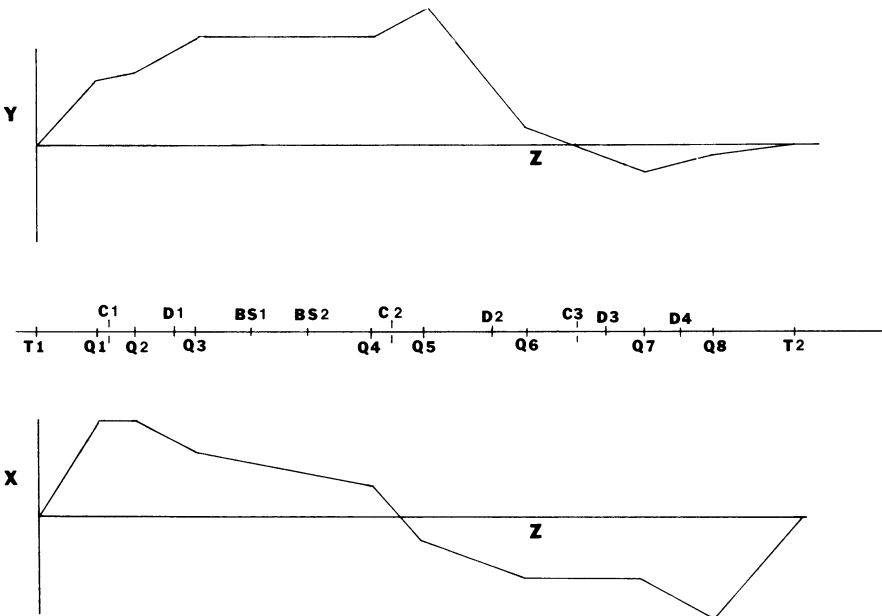
slit C3 downstream from the separators. The vertical position of the focus depends on the divergence that the particles received at the separators. The last three quadrupoles (Q6–Q8) bring the beam to a horizontal and vertical focus at the experimental target.

Now consider the profile of a beam of particles. In the 2-dimensional phase space plot the locus of the displacements and divergences at a fixed z defines an ellipse [16]. When the major axis of the ellipse is along x', the beam is said to be at a waist. This usually corresponds to a point of minimum beam size. The ratio of x to x' at a waist is defined to be the characteristic length of the beam

$$\tilde{X} = x/x' \tag{4.31}$$

The product of x and x' at a waist is known as the emittance of the beam

$$\epsilon = xx' \tag{4.32}$$

so that the area of the phase space ellipse is $\pi\epsilon$.

Let us assume that a beam that is initially at a waist, as indicated in Fig. 4.9a, enters a beamline consisting of a drift space, thin convergent lens, and another drift space. In the drift space the divergence of any particle in the beam remains constant and the phase space ellipse shears horizontally. Note that points a and b in the figure have 0 divergence initially, so their position on the figure cannot change while traversing the drift space. The ellipse at the end of the drift space is shown in Fig. 4.9b. The amount of horizontal shearing is determined by the length of the drift space. Upon crossing the thin lens the position of the particles remains the same, but all the divergences are changed by an amount given by Eq. 4.27. Thus, the phase space ellipse appears as in Fig. 4.9c. Note that points e and f, which are on the lens axis, remain fixed. Finally the second drift space shears the ellipse again horizontally and the phase space ellipse reaches another waist as shown in Fig. 4.9d (points h and i remain fixed).

One is often interested in finding the location z_2 and characteristic length $\tilde{X}_2$ of the second waist if the first drift distance z_1, the initial characteristic length $\tilde{X}_1$, and the focal length f of the lens are given. If we define the auxiliary variable

$$\rho = \frac{f^2}{\tilde{X}_1^2 + (z_1 + f)^2} \tag{4.33}$$

then the characteristic length of the outgoing beam is

$$\tilde{X}_2 = \rho \tilde{X}_1 \tag{4.34}$$

and the location of the second waist is

$$z_2 = \rho(z_1 + f) - f \tag{4.35}$$

The semiwidth or profile of the output beam is given by

$$x_2^2 = \epsilon \tilde{X}_2 (1 + (z - z_2)^2 / \tilde{X}_2^2) \tag{4.36}$$

where z is measured from the center of the lens.

In practice, it is necessary to use two or more quadrupoles to achieve simultaneous focusing in both the horizontal and vertical planes. Consider a pair of quadrupoles with powers P_1 and P_2 separated by a distance d. Then if the object is a distance u before the first quadrupole and the image is required to be a distance v beyond the second quadrupole, the transfer matrix in the focusing–defocusing (FD) plane is the product

$$M = \begin{bmatrix} 1 & v \\ 0 & 1 \end{bmatrix} \begin{bmatrix} 1 & 0 \\ P_2 & 1 \end{bmatrix} \begin{bmatrix} 1 & d \\ 0 & 1 \end{bmatrix} \begin{bmatrix} 1 & 0 \\ -P_1 & 1 \end{bmatrix} \begin{bmatrix} 1 & u \\ 0 & 1 \end{bmatrix} \tag{4.37}$$

The condition for imaging is that a given point on the object map to a given point on the image, independent of the divergence at the point on

Figure 4.9 Phase space ellipses for waist to waist beam transport.
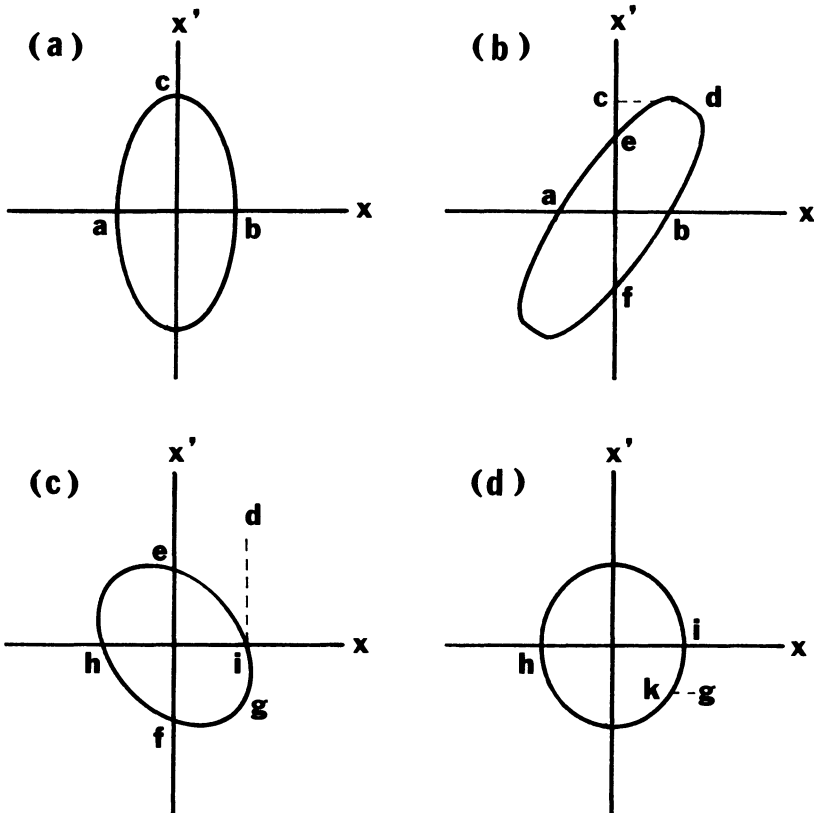
the object. This requires that $M_{12} = 0$. Developing a similar equation for the DF plane and solving for the lens power gives [16]

$$(uP_1)^2 = \frac{u + v + d}{d} \frac{u + d}{v + d}$$

$$(vP_2)^2 = \frac{u + v + d}{d} \frac{v + d}{u + d}$$

(4.38)

4.4 Flux monitors

Studies of total or differential cross sections require the measurement of the incident particle intensity. It is easy to make a relative monitor by constructing a small solid angle scintillation counter telescope. The telescope can be made more selective by incorporating range, energy loss, or time of flight requirements on the accepted particles.

In e⁺e⁻ machines the incident luminosity is determined from measurements of small angle or large angle Bhabha scattering events. The differential cross section for this process may be calculated exactly, so the number of observed events together with the known acceptance of the detectors gives an absolute measurement of the luminosity. Similarly pp or p̄p colliders can use small angle elastic scattering to determine the luminosity.

The intensity of a photon beam can be determined if two of the quantities (total energy, maximum energy, number of photons in a known energy interval) are measured [17]. For low intensity charged beams a thin scintillation counter may be used to count the incident particles. At higher intensities a pickup electrode or calibrated ionization chamber may be used to provide a signal proportional to the beam intensity. A similar technique is to use an integrating scintillation or Cerenkov counter [17]. The charge from the photomultiplier tube is collected on a capacitor. The Cerenkov counter presents more material to the beam but offers superior background rejection. For very high currents, such as with the SLAC e⁻ beam, the ionization chamber output saturates, and it is necessary to use a secondary emission monitor.

Another technique that can be useful involves a measurement of the induced radioactivity in a thin metal foil [18]. Suppose we uniformly irradiate a thin foil of some material such as aluminum or gold. The number of radioactive nuclei produced in the foil per unit volume and per unit time will be

$$n = \Phi n_a \sigma_T$$

(4.39)

where Φ is the incident flux (the number of incident beam particles per

unit area per unit time), n_a is the number of foil atoms per unit volume, and σ_T is the total cross section for producing the radioactive isotope under consideration. The number of particles produced per unit time is

$$\mathcal{N}_{\text{sat}} = \Phi \sigma_T \rho \frac{N_A}{A} \mathcal{A} d \tag{4.40}$$

where $\mathcal{A}$ is the area of the foil that is irradiated and d is the foil thickness. Now the beam intensity (number of particles per unit time) is just

$$\phi = \Phi \mathcal{A} \tag{4.41}$$

The product ρd can be conveniently measured in terms of the total mass of the foil, M_{tot}, and its total area, $\mathcal{A}_{\text{tot}}$,

$$\rho d = M_{\text{tot}} / \mathcal{A}_{\text{tot}} \tag{4.42}$$

Thus Eq. 4.40 becomes

$$\mathcal{N}_{\text{sat}} = \phi \sigma_T \frac{N_A}{A} \frac{M_{\text{tot}}}{\mathcal{A}_{\text{tot}}} \tag{4.43}$$

The activity, or number of radioactive decays per unit time, approaches $\mathcal{N}_{\text{sat}}$ exponentially since the isotope has a half-life for decaying of $t_{1/2}$. A nuclei produced at time τ has a probability $\exp[-(t_i - \tau)0.693/t_{1/2}]$ of remaining at time t_i. Let $N(t_i, t_c)$ be the number of radioactive nuclei remaining after an irradiation time t_i and a "cooling" time t_c during which it is not irradiated. The number of decaying nuclei at time t_i can be found by integrating over the contributions from all times τ

$$N(t_i, 0) = \mathcal{N}_{\text{sat}} \int_0^{t_i} \exp[-(t_i - \tau)0.693/t_{1/2}] \, d\tau$$

$$= \mathcal{N}_{\text{sat}} \frac{t_{1/2}}{0.693} (1 - e^{-0.693 t_i / t_{1/2}}) \tag{4.44}$$

If we allow the foil to cool for a time t_c, the number of radioactive nuclei will be

$$N(t_i, t_c) = \mathcal{N}_{\text{sat}} \frac{t_{1/2}}{0.693} (1 - e^{-0.693 t_i / t_{1/2}}) e^{-0.693 t_c / t_{1/2}} \tag{4.45}$$

To get the activity, we take the derivative of this with respect to t_c.

$$\mathcal{N}(t_c) = \mathcal{N}_{\text{sat}} (1 - e^{-0.693 t_i / t_{1/2}}) e^{-0.693 t_c / t_{1/2}} \tag{4.46}$$

One can measure the activity $\mathcal{N}$ of a given isotope of known half-life that has been produced in a foil irradiated for a time t_i and cooled for a time t_c. One can then determine $\mathcal{N}_{\text{sat}}$ from Eq. 4.46. Then using Eq. 4.43 and the measured properties of the foil, one can make an absolute determination of the average beam intensity ϕ.

Figure 4.10 shows the growth of activity of several isotopes produced by proton irradiation of a thin aluminum foil. Note that isotopes with short half-lives like ^{13}N saturate quickly and at a low level of total activity. Fluorine-18 is a useful isotope for intensity measurements because its half-life of 110 min is convenient for the growth of activity and because the positron emitted in its decay can easily be detected in a NaI well counter.

4.5 Other particle sources

Although most particle physics experiments utilize accelerator beams, other particle sources are sometimes used. Some experiments such as those searching for proton decays or the presence of free quarks in

Figure 4.10 Induced activities of various isotopes in aluminum as a function of the irradiation time. The curves assume the value $\rho d = 5.89$ mg/cm^2.
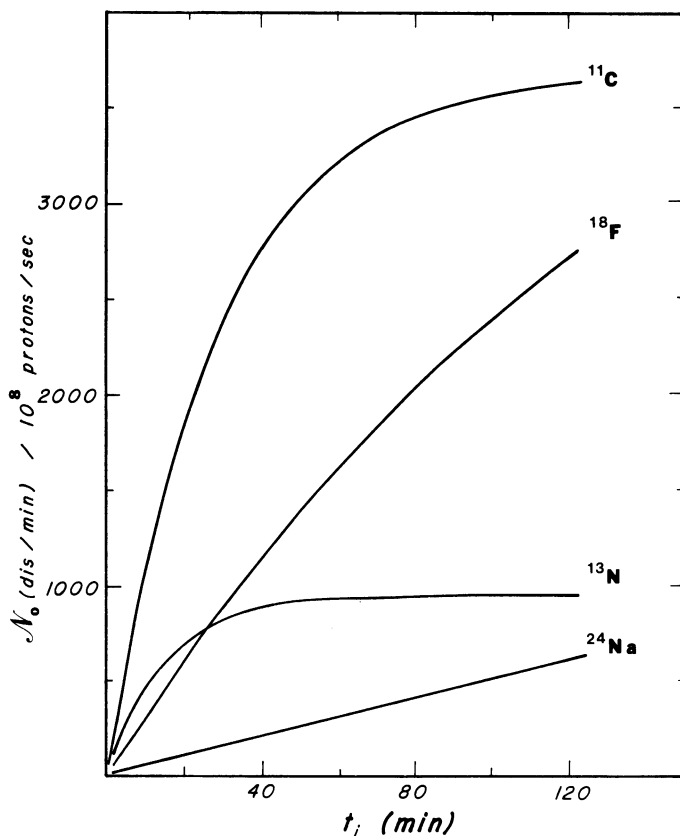
matter do not use a beam at all. Studies have been made of electron type neutrinos from the sun and $\bar{\nu}_e$ from fission reactors. Other sources of particles include cosmic rays and radioactive atoms.

In some experiments the presence of cosmic rays presents an unwanted source of background events, while for others they can be a useful tool for alignment and for checking detectors outside the beam region. The primary cosmic rays in outer space consist of protons, alpha particles, and heavier nuclei, roughly in the proportion 93 : 6 : 1. These strike particles in the upper atmosphere, producing many other elementary particles. Because of the charge imbalance of the primary particles and of the deflection of the particles in the earth's magnetic field, the intensity of various particles at sea level depends on the latitude, east – west direction, momentum interval, and angle from the vertical [19].

Cosmic ray fluxes are usually quoted in units of particles/cm²-s, which is appropriate for flat detectors sensitive to particles from many directions or in units of particles/cm²-s-sr for telescopic detectors with limited angu-

Figure 4.11 Flux of cosmic ray particles at sea level at 40° N geomagnetic latitude. The low energy electron and proton spectra can differ significantly from the dotted lines depending on local conditions in the atmosphere. (J. Ziegler, Nuc. Instr. Meth. 191: 419, 1981.)
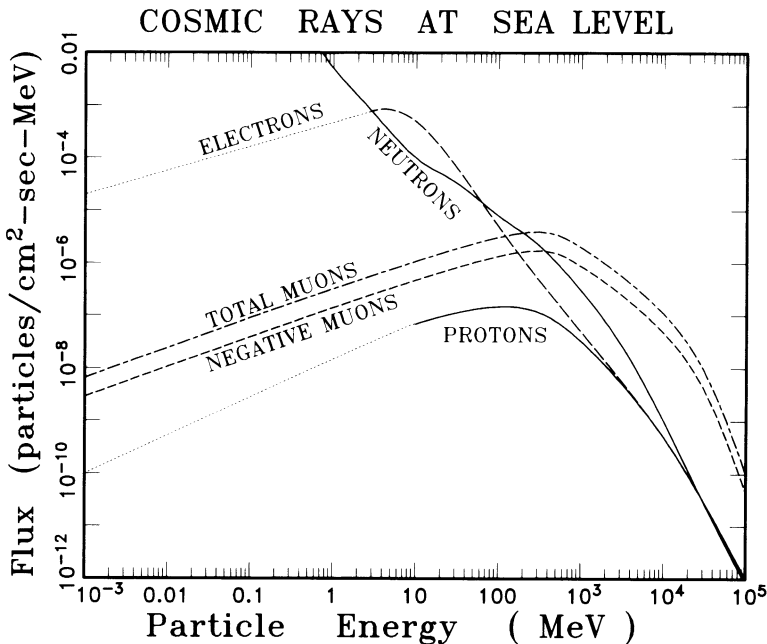
lar acceptance. The energy spectra of the main components of the cosmic ray flux at sea level are shown in Fig. 4.11. The total surface cosmic ray intensity is ~ 500 particles/m²-s for midnorthern latitudes [20]. The muon momentum spectrum peaks around 800 MeV/c. The continuous spectrum of neutrons peaks around 0.1 eV.

Radioactive sources are useful for calibration and efficiency measurements. The common unit of activity is the Curie (Ci), where

$$1 \text{ Ci} = 3.7 \times 10^{10} \text{ disintegrations/sec}$$
$$= 3.7 \times 10^{10} \text{ becquerel (Bq)}$$

The unit of exposed dose is the roentgen (R). This is defined in terms of the amount of charge of either sign present in 1 cm³ of air (STP) due to ionization or

$$1 \text{ R} = 1 \text{ esu/cm}^3$$

Table 4.4 contains a list of some radioactive sources that are useful for calibration purposes.

Table 4.4. *Radioactive sources*

Isotope	$t_{1/2}$ (yr)	Decay product	Particle energies (MeV)
^{3}H	12.26	e^-	0.019
^{22}Na	2.602	γ	0.511, 1.275
		e^+	0.54, 1.8
^{55}Fe	2.6	X-rays	0.0057
^{60}Co	5.26	β	0.315
		γ	1.173, 1.332
^{85}Kr	10.76	e^-	0.670
		γ	0.514
^{90}Sr	28.1	e^-	0.546
^{106}Ru	1.01	e^-	0.039
$\rightarrow ^{106}$Rh	30 sec	e^-	2.0, 2.4, 3.1, 3.53
		γ	0.512, 0.616
^{109}Cd	1.23	γ	0.088
^{133}Ba	7.2	γ	0.081, 0.303, 0.356
^{137}Cs	30.23	γ	0.662
		e^-	0.511, 1.176
^{207}Bi	30.2	γ	0.570, 1.064, 1.770
		β	0.481, 0.554, 0.976, 1.048
^{241}Am	458	γ	0.060
		α	5.486, 5.443, 5.389

Source: CRC Handbook of Chemistry and Physics, 64th ed., Boca Raton: CRC Press, 1983; Radioisotope data chart, Bicron Corp, Newbury, Ohio, 1974.

4.6   Radiation protection

High intensity beams of particles present a potential hazard to experimenters and to the accelerator's environment. For this reason, particle beams are shielded transversely and are terminated in massive beam dumps consisting of many interaction lengths of absorber. At energies less than 10 GeV neutrons and photons tend to be the chief components of stray radiation, while at energies above 100 GeV muons play a dominant role downstream of the target.

In health physics the common unit of absorbed energy dose in a given mass of material is the rad, where

$$
\begin{aligned}
1 \text{ rad} &= 100 \text{ ergs/g} \\
&= 6.24 \times 10^7 \text{ MeV/g} \\
&= 10^{-2} \text{ gray (Gy)}
\end{aligned}
$$

It turns out, however, that 1 rad of radiation can have a different relative biological effectiveness (RBE) depending on a number of other factors. Therefore, when discussing exposure of human tissue to radiation, the preferred unit is the rem. This stands for "roentgen equivalents for man" and is given by

$$
\begin{aligned}
1 \text{ rem} &= 1 \text{ rad} \times \text{RBE} \\
&= 10^{-2} \text{ sievert (Sv)}
\end{aligned}
$$

The RBE can depend on many factors, including the spatial distribution of the dose, dose rate, type of radiation, the type of tissue absorbing the radiation, and the energy loss per centimeter in the tissue [21]. This last quantity is particularly important and is referred to as the linear energy transfer (LET).

For radiation protection the RBE is expressed in terms of a quality factor, which is a function of the LET and takes into account how efficiently the radiation deposits energy. Quality factors vary from ~1 for photons, electrons, and minimum ionizing particles to ~20 for alpha particles and heavy ions.

Figure 4.12 shows the fluxes of several types of particles that are equivalent to an exposure of 1 mrem/hr. Note that around 1 GeV a flux of ~5 particles/cm²-s of any type gives an exposure of 1 mrem/hr. For comparison the maximum permissible dose for the whole body in the United States is 5 rem/yr. A rough estimate of the natural background radiation due to cosmic rays is ~50 mrem/yr, while that from radioactive rocks and radioactive gases in the atmosphere is ~75 mrem/yr.

Radiation can kill cells and disturb the normal functioning of organs [22]. The most susceptible tissues and organs are the bone marrow, lym-

phatic system, skin, gastrointestinal tract, gonads, thyroid, and eyes. Long
term, low level exposure to radiation can cause cancer, leukemia, and
genetic mutations. The exact effect of this type of exposure is complicated
due to the body's ability to adapt to and repair the damaged tissue. A
massive short term exposure can cause radiation sickness, involving a
serious decrease in the number of circulating blood cells. A dose of ~ 300
rem to the center of the body may be sufficient to cause death.

Particles entering a block of shielding material are attenuated exponen-
tially. High energy neutrons are primarily removed through inelastic
interactions. The attenuation of high energy particles is quite complicated
since each interaction can produce several other particles, which are
themselves capable of producing additional particles. We will discuss the
resulting formation of electromagnetic and hadronic showers in more
detail in Chapter 11. Accurate predictions of particle fluxes emerging
from a shielding block usually require Monte Carlo calculations.

Earth and concrete are commonly used as shielding materials. The
energy spectrum of the emerging particles can be strongly affected by the
chemical composition of the material. For example, earthen barriers are
more efficient at removing low energy neutrons than concrete blocks
because of the larger fraction of water.

Figure 4.12 Particle fluxes equivalent to a dose of 1 mrem/hr. (A. Rindi
and R. Thomas, adapted with permission from the Annual Review of
Nuclear Science, Vol. 23, © 1973 by Annual Reviews, Inc.)
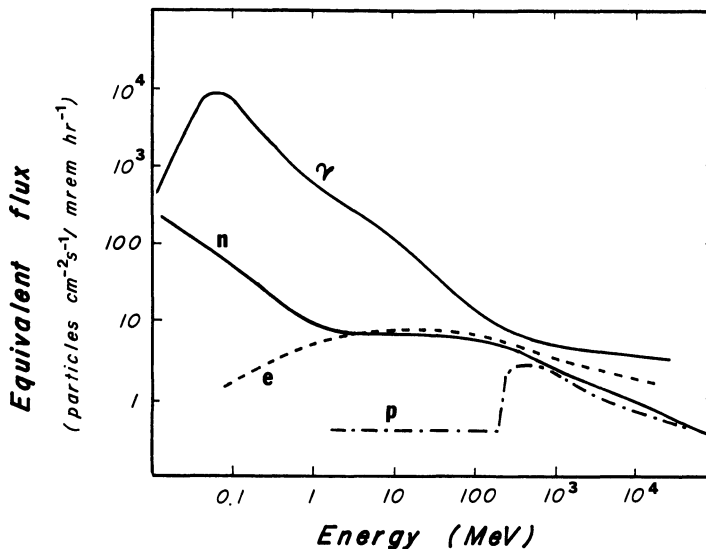
Besides the problem of stray beams there are several other environmental considerations concerning the radiation produced at an accelerator [21]. The first is radioactivity induced in accelerator components. This applies particularly to isotopes produced in plastics, oils, concrete, iron, aluminum, steel, and copper. There is a group of a few dozen isotopes whose half-lives are longer than $\frac{1}{2}$ hr, so that significant amounts may remain around long after the accelerator has been turned off. About 70% of these isotopes are γ emitters. A related nonhealth aspect of the radioactivity is radiation damage to the accelerator components. Such damage can cause failure of electronic equipment and structural weakening. Another health problem of lesser importance is the production of radioactivity in the air and in the cooling water that flows through the magnets.

References

[1] More technical details can be found in the books by E. Persico, E. Ferrari, and S. Segre, *Principles of Particle Accelerators,* Reading: Benjamin, 1968; M. Livingston and J. Blewett, *Particle Accelerators,* New York: McGraw-Hill, 1962; *Physics of High Energy Particle Accelerators,* New York: AIP, AIP Conf. Proc. Nos. 87, 105, and 127.

[2] An overview of existing and proposed high energy accelerators can be found in the review by M. Crowley-Milling, High energy particle accelerators, Rep. on Prog. Phys. 46: 51–95, 1983.

[3] J. Sanford, The Fermi National Accelerator Lab., Ann. Rev. Nuc. Sci. 26: 151–98, 1976.

[4] J. Jackson, *Classical Electrodynamics,* New York: Wiley, 1962, p. 471.

[5] R. Fernow and A. Krisch, High energy physics with polarized proton beams, Ann. Rev. Nuc. Part. Sci. 31: 107–44, 1981.

[6] R. Kohaupt and G. Voss, Progress and problems in performance of e^+e^- storage rings, Ann. Rev. Nuc. Part. Sci. 33: 67–104, 1983.

[7] E. Commins and P. Bucksbaum, The parity non-conserving e-N interaction, Ann. Rev. Nuc. Part. Sci. 30: 1–52, 1980.

[8] C. Pellegrini, Colliding beam accelerators, Ann. Rev. Nuc. Sci. 22: 1–24, 1972.

[9] F. Cole and F. Mills, Increasing the phase-space density of high energy particle beams, Ann. Rev. Nuc. Part. Sci. 31: 295–335, 1981.

[10] J. Sandweiss, Beam production at modern accelerators, in R. Shutt (ed.), *Bubble and Spark Chambers,* Vol. 2, New York: Academic, 1967, Chap. 4.

[11] D. Aston, M. Atkinson, A.H. Ball, G.R. Brookes, P.J. Bussey, B. Cake, D. Clarke, K. Connell, I.P. Duerdoth, R.J. Ellison, P.J. Flynn, W. Galbraith, P.G. Hampson, M. Ibbotson, R.E. Hughes-Jones, M.A.R. Kemp, G.D. Lafferty, J.B. Lane, J. Litt, D. Mercer, D. Newton, C. Raine, J.H.C. Roberts, K.M. Smith, K.M. Storr, R. Thompson, and A.P. Waite, The 25-70 GeV tagged photon facility at CERN, Nuc. Instr. Meth. 197: 287–96, 1982.

[12] H. Fisk and F. Sciulli, Charged current neutrino interactions, Ann. Rev. Nuc. Part. Sci. 32: 499–573, 1982.

[13] J. Drees and H. Montgomery, Muon scattering, Ann. Rev. Nuc. Part. Sci. 33: 383–452, 1983.

[14] A. Jonckheere, C. Nelson, B. Collick, S. Heppelman, Y. Makdisi, M. Marshak, E. Peterson, K. Ruddick, D. Berg, C. Chandlee, S. Cihangir, T. Ferbel, J. Huston, T.

Jensen, F. Lobkowicz, M. McLaughlin, T. Oshima, P. Slattery, and P. Thompson, Enhanced 200 GeV/c K$^+$ beam using a Be filter, Nuc. Instr. Meth. 180: 25–8, 1981.

[15] J. Lach and L. Pondrom, Hyperon beam physics, Ann. Rev. Nuc. Sci. 29: 203–42, 1979.

[16] A. Banford, *The Transport of Charged Particle Beams,* London: Spon, 1966.

[17] D. Caldwell and G. James, Beam monitoring methods, in D. Ritson (ed.), *Techniques of High Energy Physics,* New York: Interscience, 1961, Chap. 11.

[18] M. Babier, *Induced Radioactivity,* Amsterdam: North-Holland, 1969.

[19] S. Hayakawa, *Cosmic Ray Physics,* New York: Wiley, 1969.

[20] J. Ziegler, The background in detectors caused by sea level cosmic rays, Nuc. Instr. Meth. 191: 419–24, 1981.

[21] A. Rindi and R. Thomas, The radiation environment of high energy accelerators, Ann. Rev. Nuc. Sci. 23: 315–46, 1973.

[22] A. Upton, Effects of radiation on man, Ann. Rev. Nuc. Sci. 18: 495–528, 1968.

Exercises

1. Suppose that a proposed 20-TeV proton collider could be built with 2.5 T, 5.0 T, or 7.5 T bending magnets. Assuming that the dipoles fill 80% of the available space, calculate the circumferences of the corresponding tunnels. What are the synchrotron radiation losses for each case?

2. Find the equivalent CM energies for 400- and 1000-GeV fixed target accelerators.

3. What is the expected QED rate for two-muon events at LEP if the luminosity is 10^{31} particles/cm^2-s?

4. A 10-m-long electrostatic separator with a potential difference of 100 kV across a 2-cm gap is adjusted so that there is no deflection for a 5-GeV/c beam of pions. Find the spatial separation for kaons and antiprotons in the beam.

5. Derive Eqs. 4.34, 4.35, and 4.36.

6. A 2-m-long quadrupole magnet with a 20-kG pole tip field and a 10-cm-diameter aperture is used in a 20-GeV/c beamline. Calculate the beam transport matrices for this quadrupole. What are the corresponding matrices in the thin lens approximation? Find the focal length of this lens and the change in divergence for a particle 1 cm off the axis.

7. A beam with a maximum displacement of 1 cm and angular divergence of 10 mrad has a waist 5 m before the quadrupole described in exercise 6. Where is the beam waist following the

quadrupole? What is the characteristic length of the beam at the second waist?

8. Estimate the total rate of cosmic ray muons with energy greater than 10 MeV incident on a 500-cm² drift chamber oriented perpendicular to the surface of the earth.

9. Estimate the number of rads deposited by 10^{12} minimum ionizing particles passing through a cylinder of water 2 cm in diameter and 20 cm thick.